ISSN 0036-0244, Russian Journal of Physical Chemistry A, 2023, Vol. 97, No. 10, pp. 2231–2240. © Pleiades Publishing, Ltd., 2023.
Russian Text © The Author(s), 2023, published in Zhurnal Fizicheskoi Khimii, 2023, Vol. 97, No. 10, pp. 1471–1480.

PHYSICAL CHEMISTRY OF NANOCLUSTERS, SUPRAMOLECULAR STRUCTURES, AND NANOMATERIALS

Mechanosynthesis of Sulfur-Containing Silver Halide Nanocomposites in a Dimethyl Sulfoxide Medium

F. Kh. Urakaev[a,b,*] and M. M. Burkitbayev[b,]**

[a]*Sobolev Institute of Geology and Mineralogy, Siberian Branch, Russian Academy of Sciences, Novosibirsk, 630090 Russia*
[b]*Al-Farabi Kazakh National University, Almaty, 050040 Kazakhstan*
**e-mail: urakaev@igm.nsc.ru*
***e-mail: Mukhambetkali.Burkitbayev@kaznu.edu.kz*

Received April 6, 2023; revised April 17, 2023; accepted April 20, 2023

Abstract—Transformations in the S–$AgNO_3$–NH_4X–NH_4NO_3 (X = Cl, Br, I) system show that nanoparticles and nanocomposites with a controlled size of particles and content of components can be synthesized via mechanical treatment and adding small amounts of a liquid in which the precursors are soluble. Nanoparticles form in a dimethyl sulfoxide (DMSO) medium through conventional (continuous dissolution–crystallization) or reactive means (continuous dissolution of precursors and their reacting with subsequent crystallization of the target product), rather than by direct mechanical activation. The first version is used for synthesizing sulfur nanoparticles (nanosulfur); the second, for synthesizing silver halides. Sulfur-containing S/AgX nanocomposites with a controlled content of sulfur are synthesized mechanochemically. A predetermined content of nanosulfur in the nanocomposites is obtained via the dissolution–crystallization (recrystallization) of sulfur in DMSO inside a mechanochemical reactor. The proposed technical solution allows the synthesis of S/AgX nanocomposites through processing $AgNO_3$, NH_4X, and NH_4NO_3 (diluent) precursors, commercial sulfur, and small amounts of DMSO in planetary ball mills with different fittings. The water-soluble components of the product of mechanosynthesis are readily washed off.

Keywords: mechanosynthesis, sulfur, silver halides, dimethyl sulfoxide, mechanochemical recrystallization, nanoparticles, nanocomposites

DOI: 10.1134/S0036024423100254

INTRODUCTION

Many examples of mechanochemical transformation that occur upon adding small amounts of a liquid have been described in the literature. A special term—liquid assisted grinding (LAG)—has even been introduced [1–5]. The liquid typically allows the transformation and affects its rate or the composition of the product. It is more difficult to find examples where a liquid was added to control the size of particles and the composition of the product of mechanosynthesis. At the same time, the mechanisms of the effect a liquid has on mechanochemical transformation remain debatable, and they are not discussed at all in many works [6–8].

The aim of this work was not related to the well-known recrystallization that occurs during the mechanical activation of solid-phase systems [9–17]. We focused only on the possibility of synthesizing nanoparticles and nanocomposites via conventional and/or reactive recrystallization of initial crystalline precursors while they are processed in a planetary ball mill with small amounts of liquid dimethyl sulfoxide (DMSO) added as a solvent of the precursor [18].

The possibility of recrystallization when using liquids during the mechanical activation of solid-phase systems in addition to LAG, was described earlier in the literature, but in other aspects. The formation of defects in zinc oxide (ZnO) crystallites during wet grinding is thus attributed to an increase in the solubility of ZnO to a certain level and its subsequent recrystallization [19]. There are ways of synthesizing calcium carbonate nanoparticles by grinding waste shells of *Tapes japonica* mollusks in sodium hypochlorite solutions to form different $CaCO_3$ phases attributed to the mechanical activation of aragonite and the dissolution–recrystallization of calcite [20, 21]. Another approach is the mechanochemical synthesis of mordenite nanoparticles ($18SiO_2$: 12NaOH : $780H_2O$) from zeolites via recrystallization with the recovery of the crushed sample in a hydrothermal basic silicate solution [22]. Oliveira et al. [23] thus described a mechanochemical approach based on both dry and

liquid-assisted grinding to obtain new solid forms of raloxifene hydrochloride—a benzothiophene derivative with low bioavailability because of poor water solubility—which is used to treat osteoporosis. The effect solvent additives and the period of grinding have on the formation of 524T nylon ternary salt was also studied. It was found that salt forms according to a mechanism of dissolution–recrystallization while grinding with a solvent [24]. The authors of this work described the mechanism of the crystalline hydrate mechanosynthesis of nanosulfur [25] and copper sulfide nanocrystals [26, 27] from such precursors as copper acetate, sodium sulfide crystalline hydrate, citric acid, and sodium thiosulfate pentahydrate, using wear-resistant grinding media.

In this work, we focus on mechanochemical synthesis, particularly that of sulfur-containing nanocomposites of silver halides S/AgX (where X = Cl, Br, and I [28, 29]) with a controlled and adjustable sulfur content. Our aim is a systematic study of mechanochemical recrystallization to introduce it into research practice using the example of studying the S–$AgNO_3$–NH_4X–NH_4NO_3 solid phase system with small additives of solvent phase DMSO [18], which is commonly used to dissolve components of a system [30–32]. The controlled content of sulfur in S/AgX and the stabilization of the size of the formed nanoparticles are in this case ensured by the initial weight of powdered sulfur and substantial additions of a water-soluble powder diluent—an inert additive or a nontarget reaction product—to this system [33].

The approaches most similar to the proposed means of mechanochemical recrystallization are the DMSO-mediated solvothermal ways of synthesizing nanosulfur [30, 31] and S/AgX nanocomposites [28, 29, 32]. A disadvantage of these means is the impossibility of synthesizing S/AgX with a controlled content of sulfur. A predetermined content of nanosulfur in the nanocomposites is ensured by the dissolution–crystallization (recrystallization) of sulfur in the universal aprotic solvent DMSO [18] inside mechanochemical reactors [34].

EXPERIMENTAL

Materials

Dimethyl sulfoxide $(CH_3)_2SO$ with ≥99.5% content of the basic substance was purchased from BioChemica (AppliChem GmbH, Darmstadt, Germany). Silver and ammonium nitrates ($AgNO_3$, NH_4NO_3), ammonium halides (NH_4Cl, NH_4Br, NH_4I), and sulfur (S) were purchased from Sigma Aldrich (Germany). Water purified using a Smart2Pure system (Thermo Scientific, United States) was used for washing.

Sample Characterization

The phase composition of the synthesized samples, the sizes of coherent scattering regions (crystallite sizes), and lattice microdistortions were determined via X-ray diffraction (XRD) analysis on a Rigaku MiniFlex 600 diffractometer using copper radiation ($\lambda = 0.15405$ nm). The diffraction patterns were processed using the ICCD-PDF2 database, version 2016. Raman spectra of the samples were recorded on a Solver Spectrum spectrometer (NT MDT Instruments, Russia) using an 1800/500 diffraction grating that ensured a spectral resolution of 1 cm^{-1}. Vibrational modes for Raman spectroscopy were excited using a helium–neon laser with a wavelength of 633 nm. The recorded spectra were processed using the Origin Lab software.

The morphology, size, and elemental composition of nanoparticles were measured using a Quanta 200i 3D scanning electron microscope ((SEM), FEI, Netherlands) equipped with an energy dispersive X-ray spectroscopy (EDS) attachment. For analysis, a mixture composed of 1 g of a sample and 40 mL of water was treated in an ultrasonic bath for 30 min. A sample of the resulting suspension was deposited on a silicon substrate for SEM samples.

Transmission electron microscope (TEM) images of sulfur nanoparticles were recorded using a JEOL JEM-1400 TEM instrument (Japan) at an accelerating voltage of 80 kV. The shape and size of the nanoparticles were determined directly at the location of the microscope via ultrasonic dissolution of the product of mechanosynthesis with water. The resulting colloidal sulfur suspension was immediately pipetted onto a collodion-coated copper grid for TEM samples to immediately record images of the nanosulfur.

Mechanochemical Synthesis of Samples

Mechanical activation was conducted in grinding bowls of planetary ball mills Pulverisette 6 and Pulverisette 5 (Fritsch, Germany) with grinding media fittings made of tungsten carbide (250 mL of Pulverisette 6 with a single grinding bowl) and stainless steel (1-L Pulverisette 5 with four grinding bowls). Grinding was done in air using balls 10 mm in diameter at a weight ratio of 60 between the ball load (600 g) and a weighed portion of the powder mixture (10 g). The opposite rotational speeds of the carrier and the grinding bowls were 350 min^{-1}; the period of mechanical activation was 30 min. Nanosulfur (S*) and nanocomposites *y*S*/AgX (where X = Cl, Br, or I) were synthesized via mechanochemical recrystallization accord-

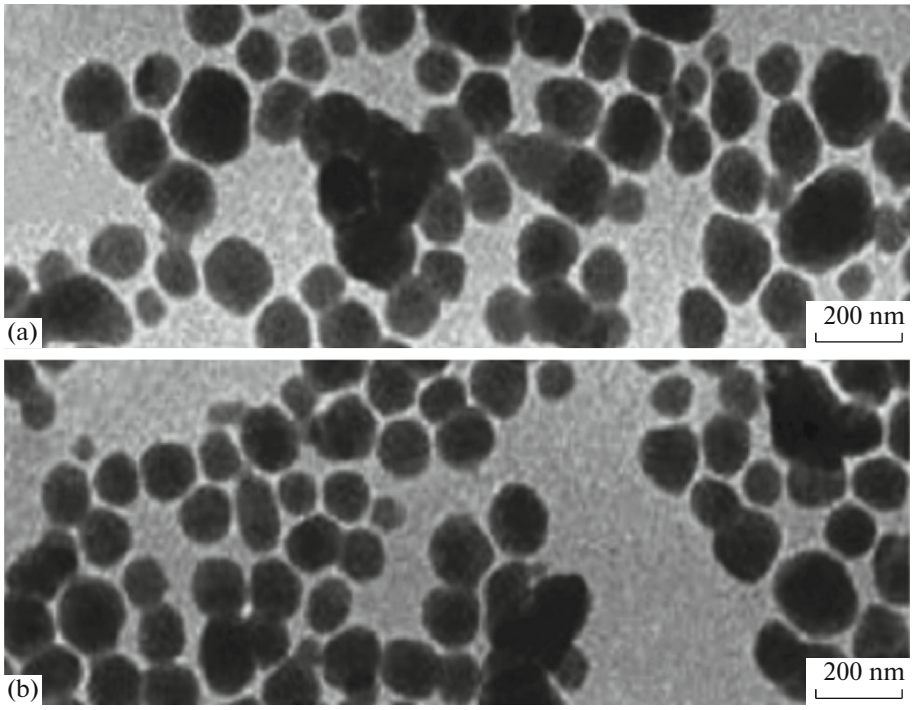

Fig. 1. Transmission electron microscope images of an aqueous suspension for our experiment on the mechanochemical recrystallization of sulfur (1 g) and ammonium iodide (NH_4I) diluent (9 g) with (a) 1 and (b) 5 mL additions of DMSO.

ing to the reactions (where S is the original sulfur, and S* is sulfur recrystallized from DMSO)

$$\begin{gathered}NH_4I\,(\text{diluent, 9 g}) + S\,(1\text{ g}) + DMSO\,(1\text{–}5\text{ mL}) \\ = NH_4I + S^* + DMSO\,(1\text{–}5\text{ mL}),\end{gathered} \quad (1)$$

$$\begin{gathered}AgNO_3 + NH_4I + zNH_4NO_3 + yS + x\text{DMSO} \\ = AgI + yS^* + (z+1)NH_4NO_3\,(\text{diluent}) + x\text{DMSO},\end{gathered} \quad (2)$$

$$\begin{gathered}AgNO_3 + NH_4X + zNH_4NO_3 + yS + x\text{DMSO} \\ = AgX + yS^* + (z+1)NH_4NO_3\ (\text{diluent}) + x\text{DMSO}.\end{gathered} \quad (3)$$

Pulverisette 6 was used for reactions (1) and (2); Pulverisette 5 was used for reaction (3). The content of yS* in S*/AgX was around 50 wt %. The advantages of the chosen reactions were the solubility of the precursors in DMSO; the absence of water (e.g., no crystalline hydrates were detected) in either the initial precursors or in the products, except for their slight moistening due to the hygroscopicity of DMSO [35–37]; and the ease, simplicity, and high rate of implementation.

The S*/AgX samples were subjected to three runs of ultrasonic washing with water to remove water-soluble components of the product of mechanosynthesis, centrifugation, and drying of the isolated target product for 24 h at 70°C. They were then studied via XRD, Raman spectroscopy, and SEM/EDS.

The gist of our approach is explained in Fig. 6. The scheme shows examples of synthesizing nanosulfur according to reaction (1) in a Pulverisette 6 mill (Fig. 6a) along with nanocomposites S*/AgI (Figs. 6b, 7) and S*/AgX (Figs. 6b, 6c) via reactions (2) and (3) in Pulverisette 6 and Pulverisette 5 mills. Figure 6c describes processes/effects that occur during and after grinding. Adding universal solvent DMSO [18] and neutral diluents (NH_4I, NH_4NO_3) ensures stabilization of the size of the resulting sulfur and silver halide nanoparticles in DMSO [31, 33].

RESULTS AND DISCUSSION

Synthesis of Nanosulfur and S/AgI Nanocomposites*

The mechanochemical recrystallization of sulfur in DMSO with inert NH_4I diluent was initially conducted according to reaction (1) to ensure the sulfur transitioned into a nanoscale state (Fig. 6a). Transmission electron microscopy images of the sulfur particles are shown in Fig. 1. The sizes of the sulfur particles lie in the range of 20–160 nm (average size, ~100 nm) and depend only slightly on the amount of DMSO. S*/AgI nanocomposites were synthesized according to a similar procedure using $AgNO_3$

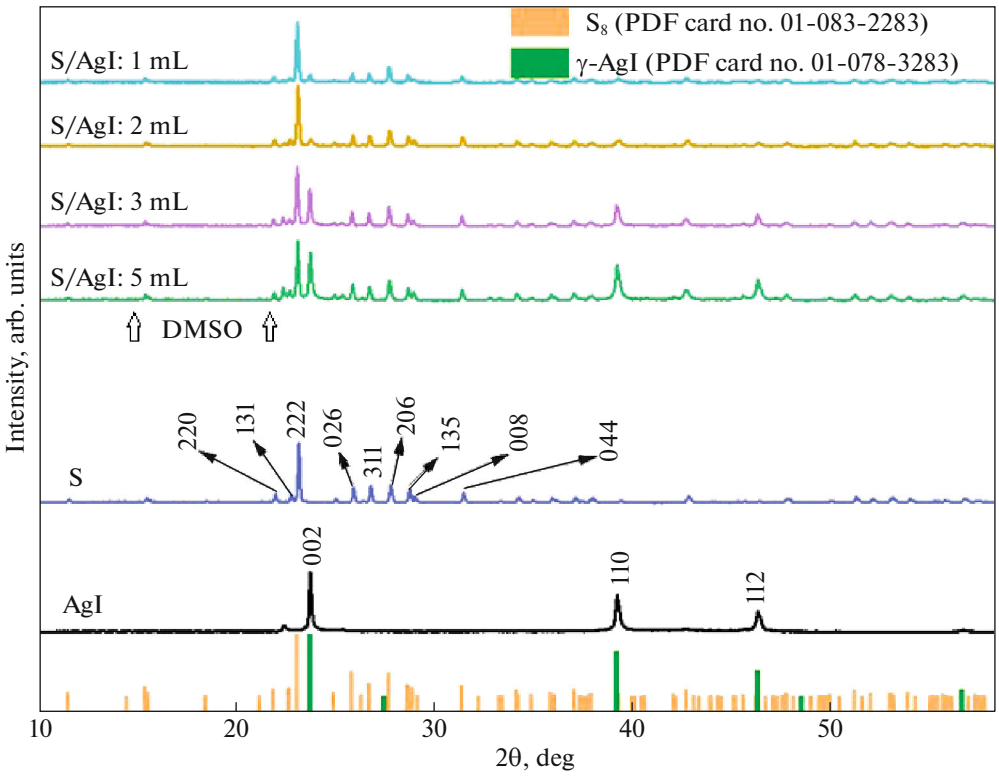

Fig. 2. Results from X-ray diffraction analysis for samples of S*/AgI nanocomposites synthesized in a Pulverisette 5 mill with 5, 3, 2, and 1 mL additions of DMSO.

(≈1.7 g), NH_4I (≈1.5 g), and NH_4NO_3 precursors (diluent ≈4.5 g), sulfur (≈2.3 g), and DMSO (1–5 mL) in Pulverisette 6 (Fig. 7) and Pulverisette 5 mills (Fig. 2).

Note the XRD data for the AgI/S* nanocomposites shown in Fig. 7. The green pointers in Fig. 7a show AgI lines attributed to the stable hexagonal β-AgI phase and the metastable cubic γ-AgI phase. The β-AgI lines dominate in Fig. 7a; the γ-AgI lines, in Fig. 7b. The main lines of sulfur shown by yellow pointers in Figs. 7a are (like those in Fig. 7b) attributed to the most stable orthorhombic α-phase of sulfur (S_8).

The processing of the XRD data using a Williamson–Hall plot [38–40] is described in Fig. 8. The graphic versions of these plots shown in Figs. 8a–8d allow us to find crystallite sizes D along the specified portions of axis y and lattice microdistortions ε from the slopes of the straight lines. The calculated values of D indicate of nanosized regions of the coherent scattering of sulfur and silver iodide particles. Those for ε also indicate a considerable defect structure due to the mechanical activation of the crystallites. The data from repeated XRD analysis (Fig. 2) agree with and supplement the results shown in Fig. 6 for the phases in S*/AgI and in Fig. 8 for D ~ 20 nm and ε ~ 0.2% (values similar to these were obtained from the XRD data for both S*/AgCl and S*/AgBr in Fig. 9). It is also evident that the amount of DMSO and replacing the mill with another had little effect on the results.

The ratio of components and the phase and elemental composition of the AgI/S* nanocomposites were also confirmed via the Raman spectroscopy data shown in Fig. 3. It is obvious there was no appreciable difference between the spectra of the samples shown in Figs. 3a and 3b. Analysis shows the samples were distinguished by lines of silver iodide [41]: a superposition peak at ~75 cm^{-1} and a peak with a small shoulder at a wave number of 105 cm^{-1}. These results are in good agreement with the data for pure AgI, for which peaks were detected at 74 and 109 cm^{-1} (Fig. 3c).

The other wave numbers in Figs. 3a and 3b of 83, 153, 219, and 474 cm^{-1} correspond to sulfur in the S_8 modification [42]. The small but pronounced peak at ≈246 cm^{-1} is attributed to the intramolecular vibrations of S_8; the peak at ≈437 cm^{-1}, to both the intermolecular vibrations of S_8 and the start of the polymerization of S_8 [42]. The four distinct peaks at 89, 158, 223, and 477 cm^{-1} in Fig. 3c are attributed to mechanically activated pure sulfur. They are shifted to 83, 153, 219, and 474 cm^{-1}, respectively, compared to the peaks in Figs. 3a and 3b.

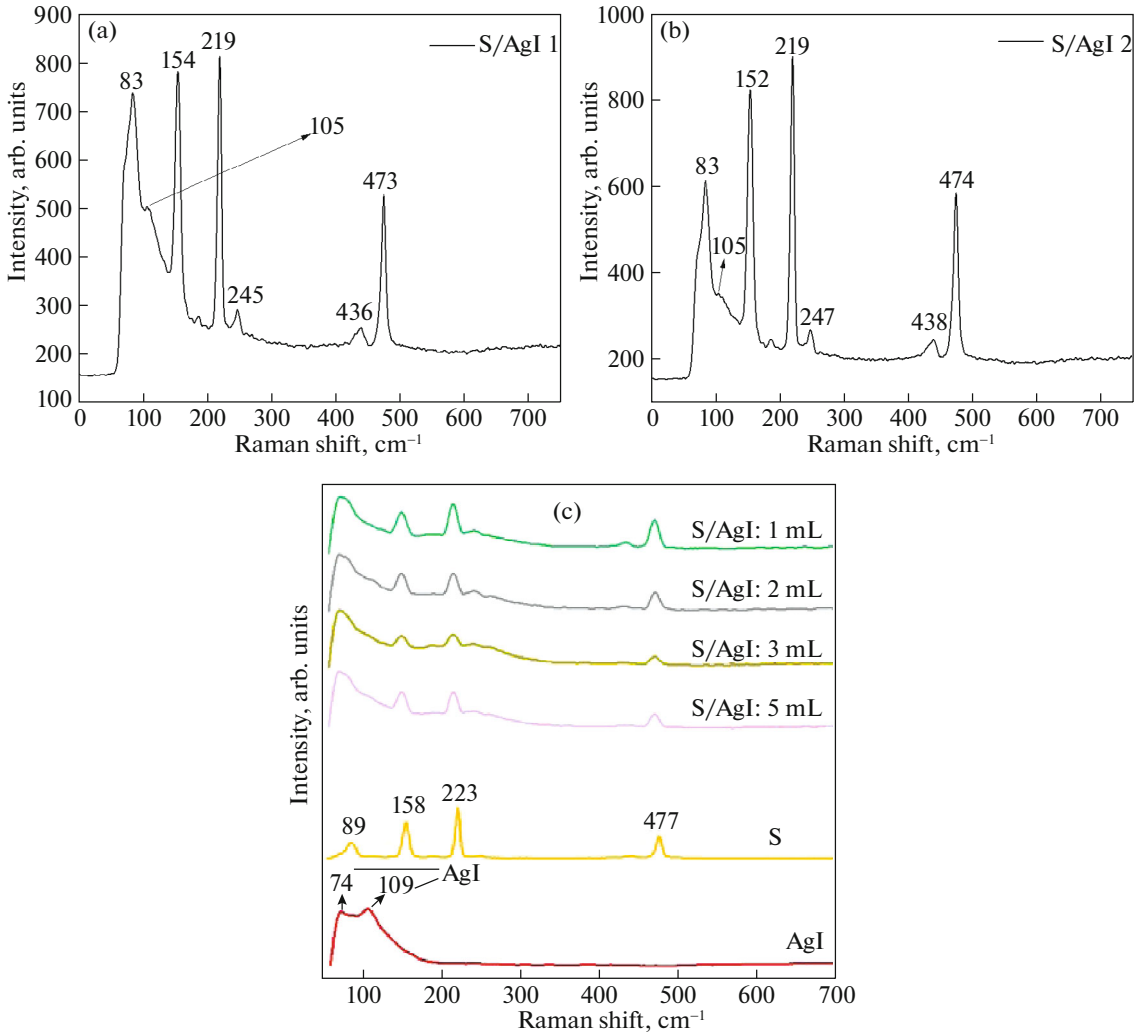

Fig. 3. Raman spectroscopy data for S*/AgI nanocomposites synthesized in a Pulverisette 6 mill with (a) 5 and (b) 1 mL additions of DMSO, and (c) in Pulverisette 5.

The morphology and particle size of S*/AgI were also measured via SEM (Figs. 4, 5a). The SEM image in Fig. 4 shows that the S*/AgI composite was composed of particles with the most diverse shapes and sizes. A more detailed and expanded analysis of this image shows that these particles were agglomerates of smaller particles and revealed nanosulfur deposits on their surfaces. The elemental composition of AgI/S* was measured using SEM/EDS (Figs. 5b, 5c); it is evident that both the intensity of the sulfur line (Fig. 5b) and the atomic content of sulfur (Fig. 5c) are similar to those for Ag and I. Analogous SEM images were recorded for S*/AgCl and S*/AgBr.

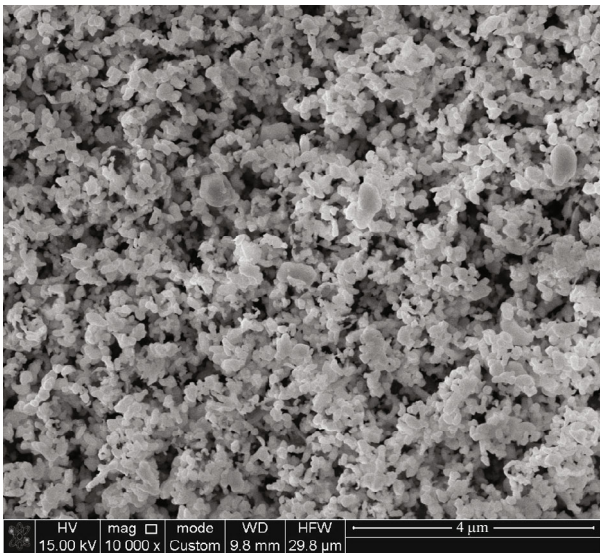

Fig. 4. Scanning electron microscope image of the S*/AgI nanocomposite synthesized with the addition of 1 mL of DMSO.

X-ray Diffraction and Raman Spectroscopy Data for S/AgCl and S*/AgBr Nanocomposites*

Results from studying S*/AgI nanocomposites synthesized according to reactions (2) and (3) in Pulverisette 6 (WC fittings) and Pulverisette 5 mills

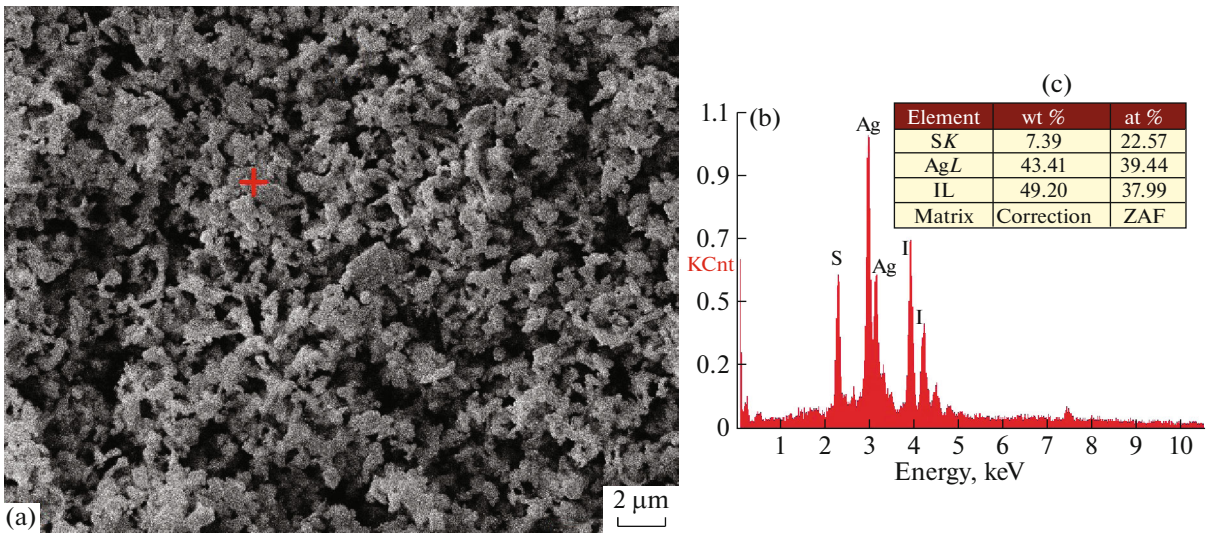

Fig. 5. (a) Scanning electron microscope image of S*/AgI synthesized with a 5 mL addition of DMSO. The area studied using EDS is marked with a cross. (b) Results from determining the elemental composition. (c) Table of element contents.

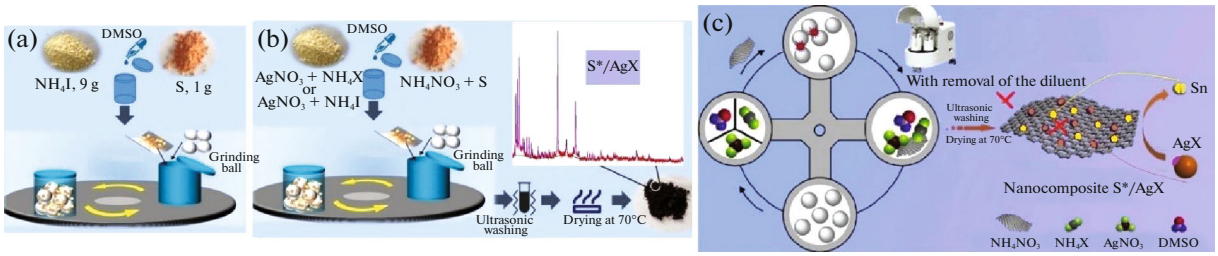

Fig. 6. Technical support for synthesizing target products according to reactions (1)–(3) via mechanochemical recrystallization in DMSO using planetary mills: (a) Pulverisette 6 for synthesizing nanosulfur using ammonium iodide as a diluent, (b) Pulverisette 6 and Pulverisette 5 for synthesizing S*/AgX or S*/AgI nanocomposites using the nontarget product of reactions (2) and (3) (ammonium nitrate) as a diluent, and (c) Pulverisette 5 for synthesizing S*/AgX nanocomposites using ultrasonic washing with water to remove water-soluble products of mechanosynthesis and drying of the target product.

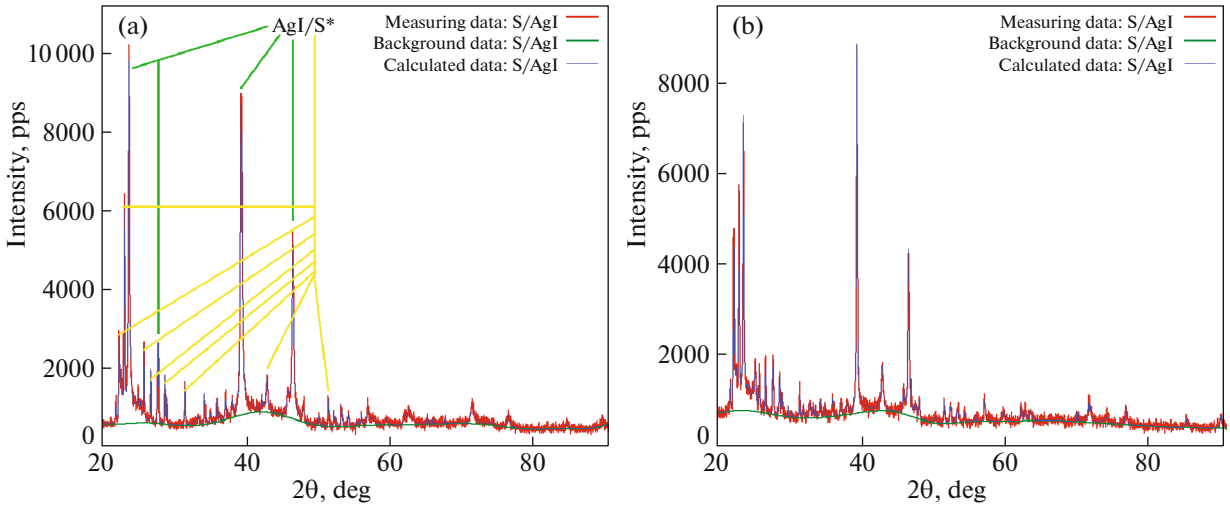

Fig. 7. Results from X-ray diffraction analysis for samples of the AgI/S* nanocomposites synthesized via mechanosynthesis with (a) 5 and (b) 1 mL additions of DMSO as specific examples of unprocessed diffraction patterns for the insets in Fig. 6b.

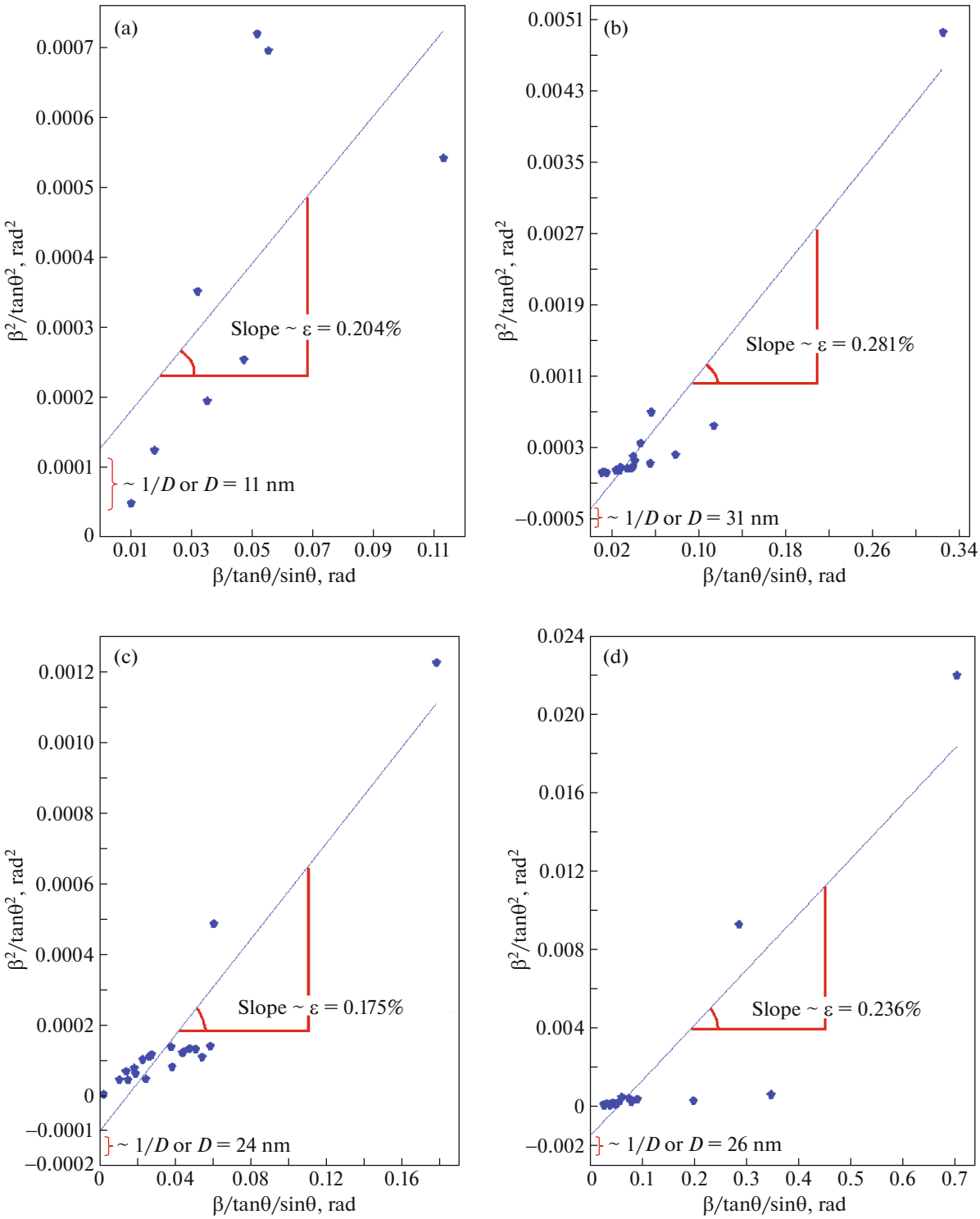

Fig. 8. Williamson–Hall plots for processing XRD data on the lines of (a, b) sulfur and (c, d) silver iodide for S*/AgX nanocomposites synthesized via mechanosynthesis with added DMSO: (a, b) 5 mL (Fig. 7a) and (c, d) 1 mL (Fig. 7b).

(Fe fittings) were discussed above. Processed XRD (Fig. 9) and Raman spectroscopy (Fig. 10) results for the reported synthesis of S*/AgI nanocomposites according to reaction (3) and/or the scheme in Fig. 6c in a Pulverisette 5 mill are given below.

XRD analysis data from S*/AgCl and S*/AgBr synthesized in DMSO (1–5 mL) for pure sulfur (α-form), and the respective cubic AgCl and AgBr phases are shown in Figs. 9a and 9b. They supplement and confirm the data shown in Figs. 2, 7, and 8.

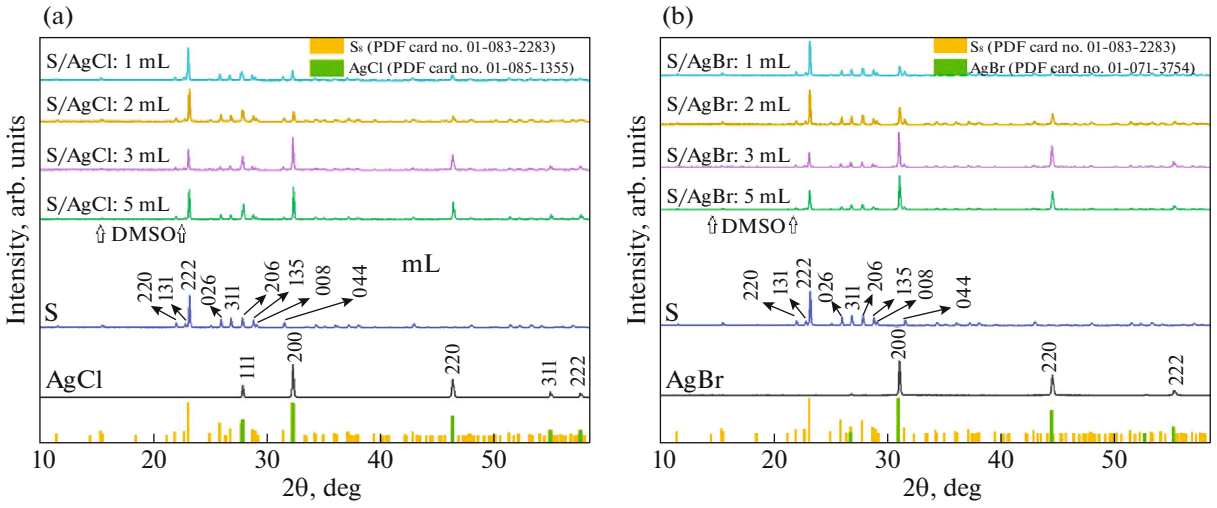

Fig. 9. Results from X-ray diffraction analysis for samples of (a) S*/AgCl and (b) S*/AgBr nanocomposites synthesized in a Pulverisette 5 mill with 5, 3, 2, and 1 mL additions of DMSO.

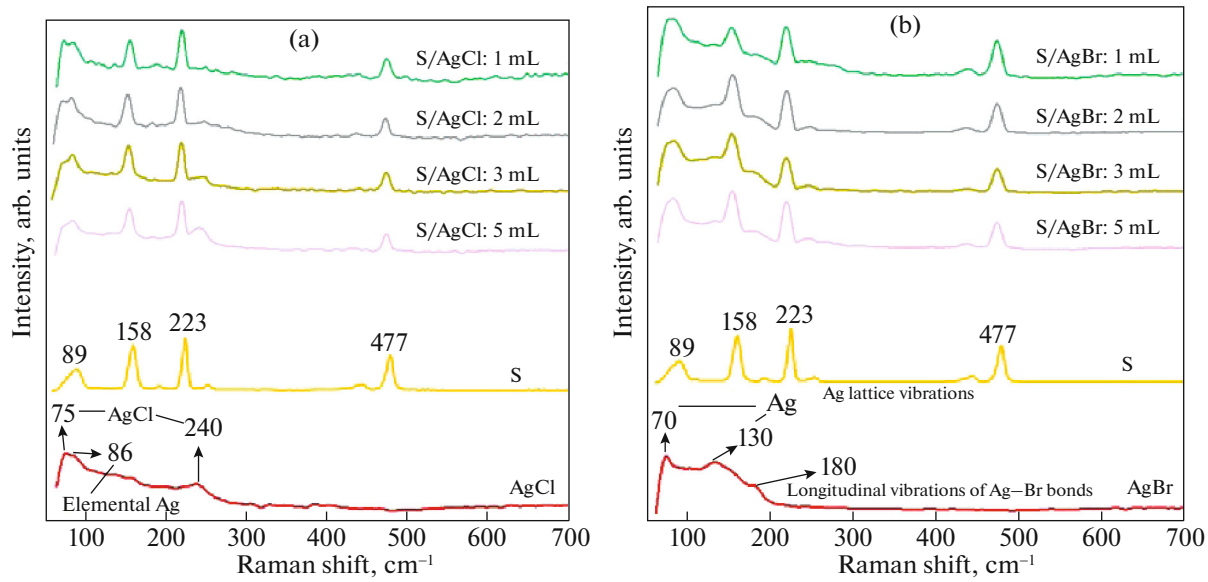

Fig. 10. Raman spectroscopy results for samples of (a) S*/AgCl and (b) S*/AgBr nanocomposites synthesized in a Pulverisette 5 mill with 5, 3, 2, and 1 mL additions of DMSO.

Note that the Raman spectra in Figs. 3 and 10 for S*/AgX always show a combination of AgX and S peaks with a constant position and considerable overlap of the peaks [28, 29, 31, 41, 42]. From the spectra of the S*/AgCl samples (Fig. 10a), three modes can be detected for pure AgCl: at 75, 86, and 240 cm^{-1}. The peaks at wave numbers of 75 and 240 cm^{-1} are attributed to AgCl, while the peak at 86 cm^{-1} is characteristic of elemental Ag, which can form under the action of a laser because of the photosensitivity and decomposition of AgCl [41]. The Raman spectra for pure AgBr (Fig. 10b) are represented by three characteristic peaks at approximately 70, 130, and 180 cm^{-1}. The peaks at 70 and 130 cm^{-1} can be attributed to the vibrations of the Ag lattice. The peak at 180 cm^{-1} is due to stretching of the Ag–Br bond. This agrees with the results for AgCl, allowing for the difference between the atomic masses.

The proposed technical solution ensures the formation of sulfur-containing S*/AgX (X = Cl, Br, I) nanocomposites via the single-stage mechanical activation of $AgNO_3$, NH_4X, and NH_4NO_3 (diluent [33]) precursors and commercial sulfur in small amounts of liquid phase DMSO, which is a universal aprotic sol-

vent for precursors [18, 31]. A predetermined content of nanosulfur in the nanocomposites is ensured by the continuous dissolution–crystallization (recrystallization) of sulfur in a DMSO medium inside mechanochemical reactors [34].

CONCLUSIONS

Mechanochemical recrystallization in solid-phase systems with small additions of liquid phase DMSO as a solvent for the precursors was thus studied systematically for the first time and introduced into research practice. The gist of this technique was explained using the example of the mechanical activation of the $S–AgNO_3–NH_4I–NH_4NO_3$ (diluent) system with variable DMSO additives resulting to the mechanosynthesis of S/AgI nanocomposites with a controlled content of nanosulfur. The content of nanosulfur in the nanocomposites for their mechanosynthesis was predetermined at a level of around 50 wt %, which was ensured by both conventional and reactive dissolution–crystallization (recrystallization) of the initial weighed portions of sulfur and precursors in DMSO. The proposed technique allows us to synthesize nanosulfur and S/AgX nanocomposites separately via single-stage mechanical treatment of an original $S–AgNO_3–NH_4X–NH_4NO_3$–DMSO system using planetary ball mills with different grinding media fittings under different conditions of activation.

The technique also includes ultrasonic washing with ultrapure water to remove the water-soluble components of the mechanosynthesis product, centrifuging, and drying the isolated target product for 24 h at a temperature of 70°C.

APPENDIX

Our supplementary information includes technical support for synthesizing the target products (nanosulfur and sulfur-containing silver halide nanocomposites (S/AgX)) via reactive mechanochemical recrystallization in small additions of a liquid (precursor solvent DMSO) using planetary ball mills. It also includes supporting data for studying the synthesized S/AgX samples via XRD analysis in combination with Williamson–Hall plots and Raman spectroscopy.

FUNDING

This work was supported by the Ministry of Science and Higher Education of the Republic of Kazakhstan, grant no. AP08855868. It was performed as part of State Task no. 122041400031-2 for the Sobolev Institute of Geology and Mineralogy, Siberian Branch, Russian Academy of Sciences.

CONFLICT OF INTEREST

The authors declare that they have no conflicts of interest.

REFERENCES

1. T. Friščić, S. L. Childs, S. A. A. Rizvi, and W. Jones, CrystEngComm. **11**, 418 (2009). https://doi.org/10.1039/B815174A
2. B. Meenatchi and V. Renuga, Chem. Sci. Trans. **4**, 577 (2015). https://doi.org/10.7598/cst2015.1028
3. P. Ying, J. Yu, and W. Su, Adv. Synth. Catal. **363**, 1246 (2021). https://doi.org/10.1002/adsc.202001245
4. P. A. Zaikin, O. T. Dyan, I. R. Elanov, and G. I. Borodkin, Molecules **26**, 5756 (2021). https://doi.org/10.3390/molecules26195756
5. A. Kosimov, G. Yusibova, J. Aruväli, et al., Green Chem. **24**, 305 (2022). https://doi.org/10.1039/D1GC03433B
6. E. Boldyreva, Chem. Soc. Rev. **42**, 7719 (2013). https://doi.org/10.1039/C3CS60052A
7. A. A. Michalchuk, E. V. Boldyreva, A. M. Belenguer, et al., Front. Chem. **9**, 685789 (2021). https://doi.org/10.3389/fchem.2021.685789
8. E. V. Boldyreva, Faraday Discuss. **241**, 9 (2023). https://doi.org/10.1039/D2FD00149G
9. M. Matsuoka and K. Danzuka, J. Chem. Eng. Jpn. **42**, 393 (2009). https://doi.org/10.1252/jcej.09we068
10. P. Baláž, M. Achimovičová, M. Baláž, et al., Chem. Soc. Rev. **42**, 7571 (2013). https://doi.org/10.1039/C3CS35468G
11. A. Katsenis, A. Puškarić, V. Štrukil, et al., Nat. Commun. **6**, 6662 (2015). https://doi.org/10.1038/ncomms7662
12. F. Kh. Urakaev, N. V. Khan, Zh. S. Shalabaev, B. B. Tatykaev, R. K. Nadirov, and M. M. Burkitbaev, Colloid J. **82**, 76 (2020). https://doi.org/10.1134/S1061933X20010160
13. D. Nieto-Castro, F. A. Garcés-Pineda, A. Moneo-Corcuera, et al., Inorg. Chem. **59**, 7953 (2020). https://doi.org/10.1021/acs.inorgchem.9b03284
14. G. T. M. Kadja, T. R. Suprianti, M. M. Ilmi, et al., Microporous Mesoporous Mater. **47**, 110550 (2020). https://doi.org/10.1016/j.micromeso.2020.110550
15. V. V. Zyryanov, S. A. Petrov, and A. S. Ulihin, Ceram. Int. **47**, 29499 (2021). https://doi.org/10.1016/j.ceramint.2021.07.118
16. V. V. Zyryanov, Solid State Ionics **383**, 115987 (2022). https://doi.org/10.1016/j.ssi.2022.115987
17. R. Dubadi, S. D. Huang, and M. Jaroniec, Materials **16**, 1460 (2023). https://doi.org/10.3390/ma16041460
18. M. M. Burkitbayev and F. Kh. Urakaev, J. Mol. Liq. **316**, 113886 (2020). https://doi.org/10.1016/j.molliq.2020.113886
19. G.-X. Du, Q. Xue, H. Ding, and Z. Li, Int. J. Min Process. **141**, 15 (2015). https://doi.org/10.1016/j.minpro.2015.06.008
20. J. Lu, Z. Lu, X. Li, et al., J. Clean Prod. **92**, 223 (2015). https://doi.org/10.1016/j.jclepro.2014.12.093

21. J. Lu, X. Cong, Y. Li, et al., J. Clean Prod. **172**, 1978 (2018). https://doi.org/10.1016/j.jclepro.2017.11.228
22. T. Kurniawan, O. Muraza, A. S. Hakeem, and A. M. Al-Amer, Cryst. Growth Des. **17**, 3313 (2017). https://doi.org/10.1021/acs.cgd.7b00295
23. Y. S. de Oliveira, A. C. Oliveira, and A. P. Ayala, Eur. J. Pharm. Sci. **114**, 146 (2018). https://doi.org/10.1016/j.ejps.2017.11.028
24. P. Yang, X. Li, Z. Li, et al., ACS Sustain Chem. Eng. **10**, 3513 (2022). https://doi.org/10.1021/acssuschemeng.1c07869
25. F. Kh. Urakaev, A. I. Bulavchenko, B. M. Uralbekov, et al., Colloid J. **78**, 210 (2016). https://doi.org/10.1134/S1061933X16020150
26. Zh. Shalabayev, M. Baláž, N. Daneu, et al., ACS Sustain. Chem. Eng. **7**, 12897 (2019). https://doi.org/10.1021/acssuschemeng.9b01849
27. Zh. S. Shalabaev, F. Kh. Urakaev, M. Balazh, et al., Kazakh. Patent on Useful Model No. 5287, Byull. No. 32 (2020). https://gosreestr.kazpatent.kz/Utilitymodel/DownLoadFilePdf?patentId=326616&lang=ru.
28. N. Khan, M. Baláž, M. Burkitbayev, et al., Appl Surf Sci. **601**, 154122 (2012). https://doi.org/10.1016/j.apsusc.2022.154122
29. N. V. Khan, M. Baláž, M. M. Burkitbayev, et al., Int. J. Biol. Chem. **15**, 79 (2022). https://doi.org/10.26577/ijbch.2022.v15.i1.09
30. F. Kh. Urakaev, M. M. Burkitbaev, B. M. Uralbekov, and Zh. S. Shalabaev, Euraz. Patent No. 033075, Byull. No. 2019-08 (2019). https://www.eapo.org/ru/publications/publicat/viewpubl.phpıd=033075; http://www.eapatis.com/Data/EATXT/eapo2019/PDF/201700540.pdf.
31. F. Kh. Urakaev, M. M. Burkitbayev, and N. V. Khan, Int. J. Biol. Chem. **15**, 54 (2022). https://doi.org/10.26577/ijbch.2022.v15.i2.09
32. M. M. Burkitbaev, N. V. Khan, M. S. Madikasimova, et al., Kazakh. Patent on Useful Model No. 5241, Byull. No. 30 (2020). https://gosreestr.kazpatent.kz/Utilitymodel/DownLoadFilePdf?patentId=325175&lang=ru.
33. F. Kh. Urakaev, Mendeleev Commun. **22**, 215 (2012). https://doi.org/10.1016/j.mencom.2012.06.016
34. F. Kh. Urakaev, Mendeleev Commun. **26**, 546 (2016). https://doi.org/10.1016/j.mencom.2016.11.030
35. R. G. LeBel and D. A. I. Goring, J. Chem. Eng. Data **7**, 100 (1962). https://doi.org/10.1021/je60012a032
36. R. Ellson, R. Stearns, M. Mutz, et al., Combust. Chem. High throughput Screen **8**, 489 (2005). https://doi.org/10.2174/1386207054867382
37. T. J. Waybright, J. R. Britt, and T. G. McCloud, J. Biomol. Screen **14**, 708 (2009). https://doi.org/10.1177/1087057109335670
38. M. Rabiei, A. Palevicius, A. Dashti, et al., Materials (Basel) **14**, 2949 (2021). https://doi.org/10.3390/ma14112949
39. B. Himabindu, N. S. M. P. Latha Devi, and B. Rajini Kanth, Mater. Today: Proc. **47**, 4891 (2021). https://doi.org/10.1016/j.matpr.2021.06.256
40. M. P. Tirpude and N. T. Tayade, Preprint (2022). https://doi.org/10.21203/rs.3.rs-1586320/v1
41. M. Assis, F. C. Groppo Filho, D. S. Pimentel, et al., Chem. Sel. **5**, 4655 (2020). https://doi.org/10.1002/slct.202000502
42. C. Nims, B. Cron, M. Wetherington, et al., Sci. Rep. **9**, 7971 (2019). https://doi.org/10.1038/s41598-019-44353-6

Translated by M. Timoshinina